sciendo
Power Electronics and Drives
Volume 9(44), 2024 DOI: 10.2478/pead-2024-0024

Super-Twisting MRAS Observer-Based Non-linear Direct Flux and Torque Control for Induction Motor Drives

Special issue paper

Abdelkarim Ammar[1,2,*], Oussama Belaroussi[2], Meryem BENAKCHA[3], Abderrahim Zemmit[4], Tarek Ameid[5]

[1]*Institute of Electrical and Electronic Engineering, University of M'hamed BOUGARA of Boumerdes, Boumerdes, Algeria.*
[2]*LGEB Laboratory, Electrical Engineering Department, Biskra University, Algeria*
[3]*Barika University Center, Batna, Algeria*
[4]*M'sila University, M'sila, Algeria*
[5]*Faculty of Applied Science, Univ. Artois, EA 4025 LSEE F-62400, Béthune, France*

Received: 08 April 2024; Accepted: 31 May 2024

Abstract: This research paper proposes a novel design of an efficient combined sliding mode observer (SMO) for induction motor flux and speed estimation. The suggested sensorless technique employs the sliding mode's second-order approach using a model reference adaptive system (MRAS). The second-order super-twisting control method is free-chattering, which lowers the chattering effect while preserving the same good features as the first-order sliding mode control (SMC). In addition, the conjunction with the MRAS as a separated speed estimator can raise the accuracy and make the observer immune to speed fluctuations, particularly for low-speed applications. Furthermore, in order to achieve effective decoupled flux–torque control, the super-twisting algorithm (STA) was combined with a non-linear feedback linearisation controller for the inner control loop construction. This strategy can boost the control system's stability and robustness against external disturbances and modelling uncertainty. The performance analysis of the suggested methods has been carried out via simulation and experimental validation utilizing MATLAB/Simulink with the dSpace 1104 real-time interface.

Keywords: *induction motor • sliding mode observer • super-twisting algorithm • model reference adaptive system • feedback linearisation • dSpace 1104*

1. Introduction

In industrial areas, high-performance variable frequency drives are widely utilised. Commonly, scalar and vector controls are employed. In contrast to the scalar control, the vector control techniques such as field-oriented control (FOC) or direct torque control (DTC) provide quick dynamics and promising properties (Vajsz et al., 2019). Typically, the execution of closed-loop motor control systems requires accurate measurement of feedback quantities such as rotor speed, flux, and electromagnetic torque, which is achieved through the use of specific sensors. Given that sensors can be expensive and fragile, it is recommended to replace or support them with sensorless techniques.

In AC electric drive applications, sensorless control occupies an essential part. It has the potential to considerably lower the overall cost and size of the control system while increasing its efficiency. Sensorless control may be categorised into two kinds. Model-based observers and estimators, and signal injection-based techniques (Huang et al., 2021). Signal injection methods make use of rotor slot harmonics, inductance saturation, and rotor slot

* *Email: a.ammar@univ-boumerdes.dz*

leakage. These methods provide exceptional speed estimate accuracy and stability at extremely low speeds (Tang et al., 2017). However, signal injection-based techniques are difficult to deploy and they are constrained for certain industrial applications (Li et al., 2023). On the other hand, there are the soft-sensors that adopt the mathematical model. Various estimators and observers have been proposed in this context such as full-order observers (Xin et al., 2017), model reference adaptive systems (MRASs; Guedida et al., 2024) and sliding mode observers (SMOs; Qian et al., 2024).

Sliding mode control (SMC) is well known in automation for its excellent dynamic capabilities, strong resilience and straightforward design. Additionally, the sliding mode approach has confirmed its effectiveness in applications of sensorless controls as well (Czyżniewski and Łangowski, 2024; Qian et al., 2024). Compared with other observers, SMOs exhibit superior resistance to uncertainties in modelling due to their inherent variable structure control, resulting in enhanced robustness (Wu et al., 2021). Various architectures of SMOs have been presented within the last decade for speed and flux determination. In Barambones et al. (2014), to calculate rotor speed, flux, and load torque, an adaptive SMO is provided. In Lascu et al. (2009), a simpler SMC scheme is provided. In a wide-speed-range operation, this observer reduces the design complexity and increases accuracy by not taking the rotor speed into account as an adaptive quantity. Nevertheless, it makes use of a rotor flux derivative-based open loop speed estimator, which is especially prone to noise. In Mao et al. (2020), for IMs (induction motors) operating at high speeds, an improved SMC controller and observer are described; however, they have a significant chattering impact. Typically, mid-and high-speed ranges are where speed sensorless drives perform the best, but at very low speeds, particularly around zero frequency, they are not precise or durable. In Sami et al. (2020), to perform the speed-estimation process, a first-order SMO has been coupled to an MRAS estimator, where the MRAS reference voltage model will be replaced with the stator flux SMO. This relationship reduces the observer's noise sensitivity and increases the estimating accuracy in low-speed revision.

Nevertheless, the switching control in first-order SMOs excites the problem chattering, which is the fundamental drawback of SMCs (Mao et al., 2020). Higher-order derivatives of a sliding surface are used in the higher order SMCs, which is an extension of the first-order method. This provides good robustness and a free chattering control law (Sami et al., 2020). The continuous super-twisting method is capable of solving this problem while maintaining the essential properties of the standard SMC (Czyżniewski and Łangowski, 2024). Furthermore, the super-twisting algorithm (STA) does not need to compute the second derivatives of the sliding surface. This makes it a simpler choice rather than the other high-order sliding mode techniques (Holakooie et al., 2019). In Mao et al. (2020), an induction motor's speed is estimated using a fractional order super-twisting observer. However, the design of a fractional-order controller is not straightforward, as the observer gains tuning suffers from a conflict between chattering and transient performance. A sliding mode of the second order, the use of MRAS observer-based linear IM drivers is recommended also in Wang et al. (2018b).

Classical vector control approaches have limited performance due to the use of linear proportional-integral (PI) controllers that are sensitive when dealing with different uncertainties (Wang et al., 2018a,b). Therefore, several approaches in the automatic and electrical drive domains have been presented and these help achieve effective robust control, such as backstepping control feedback linearisation (Csizmadia and Kuczmann 2023). Model-based feedback linearisation is a method that can achieve decoupled control by transforming a non-linear system into an equivalent linear system. However, this technique is quite delicate because of the model uncertainties. In order to provide decoupled and robust control against parameters perturbation, inner-loop controllers for torque and flux controllers are used. The conjunction of the feedback linearisation with other robust controllers can show promising performances. This research work merges the STA on the resultant linearised system so as to mend the shortcomings of the feedback linearisation as mentioned in Ammar et al. (2020a). However, this work has extended the analyses and the comparisons with classical observers' structures.

The present paper proposes a second-order super-twisting observer connected with the MRAS. The super-twisting-based observer decreases the noise sensitivity significantly and improves the speed-estimation accuracy at low speeds. Besides, for achieving effective flux- and torque-decoupled control in the inner loops, a super-twisting feedback linearisation (STFL) controller has been designed. This combination is competent for confronting the numerous problems that arise during motor operation. By carrying out simulations and experimental validations using MATLAB/Simulink and the dSpace 1104 real-time interface, the suggested dual non-linear sensorless control's performance has been evaluated.

2. Induction Motor Modelling

Within the fixed reference frame, the induction motor's dynamic equations are given in Eq. (1):

$$\begin{cases} \dot{i}_{s\alpha} = -\mu i_{s\alpha} - \omega_r i_{s\beta} + \frac{1}{\sigma L_r}\left(\frac{\psi_{s\alpha}}{T_s} + \omega_r \psi_{s\beta}\right) + \frac{V_{s\alpha}}{\sigma L_s} \\ \dot{i}_{sb} = -\mu i_{s\beta} + \omega_r i_{s\alpha} + \frac{1}{\sigma L_r}\left(\frac{\psi_{s\beta}}{T_s} - \omega_r \psi_{s\alpha}\right) + \frac{V_{s\beta}}{\sigma L_s} \\ \dot{\psi}_{s\alpha} = V_{s\alpha} - R_s i_{s\alpha} \\ \dot{\psi}_{sb} = V_{s\beta} - R_s i_{s\beta} \\ \dot{\omega}_r = \frac{1}{J}(T_e - T_L) - \frac{f_r \omega_r}{J} \end{cases} \tag{1}$$

where:

$i_{s\alpha}$ and $i_{s\beta}$ are, correspondingly, stator current elements,
$\psi_{s\alpha}$ and $\psi_{s\beta}$ are, consequently, stator flux elements,
R_s and R_r are, correspondingly, stator and rotor resistances,
L_s and L_r are, correspondingly, stator and rotor inductances,
$T_s = L_s/R_s$ is the stator time constant,
ω_r is the rotor's speed,
T_L is the torque generated by the load,
J is an instant of inertia, and
f_r is the coefficient of friction.

$$\mu = \frac{1}{\sigma}\left(\frac{R_r}{L_r} + \frac{R_s}{L_s}\right)$$

$$\sigma = 1 - \frac{M_{sr}}{L_s L_r}$$

is the stator time constant.

M_{sr} is the inductance shared by the stator and rotor.

The equation used for electromagnetic torque is:

$$T_e = p(\psi_{s\alpha} i_{s\beta} - \psi_{s\beta} i_{s\alpha}) \tag{2}$$

p is the quantity of paired poles.

3. The super-twisting observer design with MRAS

3.2. Super-twisting algorithm

Compared to the previous high-order SMC algorithms, the STA has the advantage of not requiring the temporal derivatives of a variable that slides (Bendjeddou et al., 2021). By using only the data on the sliding surface, this method may provide a continuous control rule. This is how the super-twisting $u_{ST}(t)$ control law is put together.

$$u_{ST} = u_1(t) + u_2(t) \tag{3}$$

where:

u_{ST} is the super twisting control law, u_1 and u_2 are defined in the next expression:

$$\begin{cases} u_1 = -\lambda |S|^{\rho} \, sign(S) + \dot{u}_2 \\ u_2 = -\int \beta sign(S) \end{cases} \tag{4}$$

where S is the surface that slides, λ and β are positive gains and ρ lies in the fractional coefficient range of 0–0.5 (Rashed et al., 2005)

The sufficient requirements for STA's finite-time convergence, as stated by Levant (2003) are:

$$\begin{cases} \beta > C \\ \lambda^2 > \dfrac{4C(\beta + C)}{(\beta - C)} \end{cases} \tag{5}$$

where C is the Lipschitz's constant.

These conditions are essential for the finite-time convergence of STA. They might not be sufficient, though. Thus, Moreno and Osorio (2012) describe a stringent Lyapunov function to achieve the stability of the super-twisting method.

The controller gains, denoted as λ and β, serve two essential purposes: controller functionality and anti-disturbance capability. β is derived from the disturbance bounds, and it ensures system stability by constraining the impact of external disturbances. On the other hand, λ aligns the system with performance specifications, particularly achieving the desired reaching speed (Choi et al., 2022).

3.2. Proposed super-twisting flux observer design

The SMOs have several benefits, including great robustness, simplicity in construction, and minimal processing requirements, which allow them to function very well.

A current observer may be created by using the STA with the IM model Eq. (1) as given below:

$$\begin{cases} \dot{\hat{i}}_{s\alpha} = -\mu \hat{i}_{s\alpha} - \hat{\omega}_r \hat{i}_{s\beta} + \dfrac{1}{\sigma L_r}\left(\dfrac{\hat{\psi}_{s\alpha}}{T_s} + \hat{\omega}_r \hat{\psi}_{s\beta}\right) + \dfrac{V_{s\alpha}}{\sigma L_s} + u_1(\mathrm{S}_{\mathrm{is}\alpha}) \\ \dot{\hat{i}}_{sb} = -\mu \hat{i}_{s\beta} + \omega_r \hat{i}_{s\alpha} + \dfrac{1}{\sigma L_r}\left(\dfrac{\hat{\psi}_{s\beta}}{T_s} - \hat{\omega}_r \hat{\psi}_{s\alpha}\right) + \dfrac{V_{s\beta}}{\sigma L_s} + u_1(\mathrm{S}_{\mathrm{is}\beta}) \end{cases} \tag{6}$$

The selected switching surfaces Si in this suggested second-order SMO are stator current estimation errors.

$$\begin{cases} \mathrm{S}_{\mathrm{is}\alpha} = i_{\mathrm{s}\alpha} - \hat{i}_{\mathrm{s}\alpha} \\ \mathrm{S}_{\mathrm{is}\beta} = i_{\mathrm{s}\beta} - \hat{i}_{\mathrm{s}\beta} \end{cases} \tag{7}$$

Thus, one definition for the flux observer is:

$$\begin{cases} \hat{\psi}_{s\alpha} = V_{s\alpha} - R_s i_{s\alpha} + u_2(\mathrm{S}_{\mathrm{is}\alpha}) \\ \hat{\psi}_{sb} = V_{s\beta} - R_s i_{s\beta} + u_2(\mathrm{S}_{\mathrm{is}\beta}) \end{cases} \tag{8}$$

where u_1 and u_2 are extra design factors that are described as:

$$\begin{cases} u_1 = -\lambda |S|^{\rho} \, sign(S_{is}) \\ u_2 = -\int \beta sign(S_{is}) \end{cases} \tag{9}$$

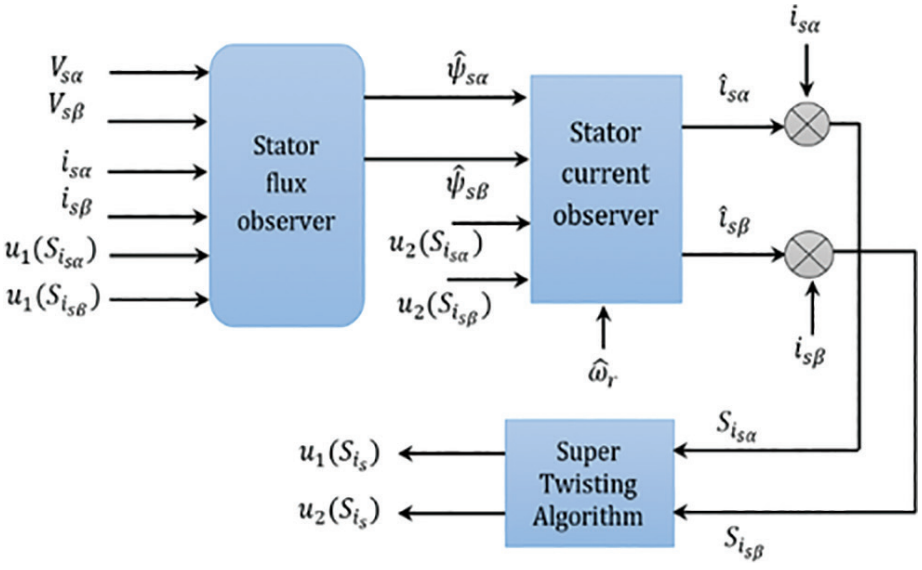

Figure 1. Current and flux observer based on super twisting.

The architecture of the suggested observer is depicted in the schematic in Figure 1.

3.3. MRAS speed estimation

In our investigation, the MRAS technique is applied to estimate the speed of the suggested observer. According to Tarchala and Orlowska-Kowalska (2018), the MRAS structure consists of the adaptation mechanism, the reference model, and the adaptive model or two sections. The proposed super-twisting observer serves as a reference model in this investigation. The computed flux quantities and those produced by the adaptive model of the MRAS will next be compared.

The adaptable model is written as follows:

$$\begin{cases} \tilde{\psi}_{s\alpha} = \dfrac{L_r}{R_r + L_r s}\left(\sigma L_s \hat{\omega}_r i_{s\beta} + \dfrac{L_s}{L_r}\left(R_r + \sigma L_r s\right) i_{s\alpha} - \hat{\omega}_r \tilde{\psi}_{s\beta}\right) \\ \tilde{\psi}_{s\beta} = \dfrac{L_r}{R_r + L_r s}\left(\sigma L_s \hat{\omega}_r i_{s\alpha} + \dfrac{L_s}{L_r}\left(R_r + \sigma L_r s\right) i_{s\beta} - \hat{\omega}_r \tilde{\psi}_{s\alpha}\right) \end{cases} \tag{10}$$

where *s* is the Laplace operator.

The following may be used to calculate the error between the adaptive model and the estimated quantities using the ST-observer reference:

$$\begin{cases} \varepsilon_\alpha = \hat{\psi}_{s\alpha} - \tilde{\psi}_{s\alpha} \\ \varepsilon_\beta = \hat{\psi}_{s\beta} - \tilde{\psi}_{s\beta} \end{cases} \tag{11}$$

To generate the predicted speed quantity, the error is used to power a suitable adaption mechanism (Schauder, 1992). The following state error equations are generated by deducting the adjustable model from those given by the SMO:

$$\begin{bmatrix} \dot{\varepsilon}_\alpha \\ \dot{\varepsilon}_\beta \end{bmatrix} = \begin{bmatrix} -\dfrac{1}{T_r} & -\omega_r \\ \omega_r & -\dfrac{1}{T_r} \end{bmatrix} \begin{bmatrix} \varepsilon_\alpha \\ \varepsilon_\beta \end{bmatrix} + \begin{bmatrix} -\hat{\psi}_{s\beta} & \sigma L_s i_{s\beta} \\ \hat{\psi}_{s\beta} & -\sigma L_s i_{s\alpha} \end{bmatrix} \left(\omega_r - \hat{\omega}_r\right) \tag{12}$$

Eq. (12) can be expressed as:

$$[\dot{\varepsilon}] = [A][\varepsilon] + [W] \tag{13}$$

The system is assured of hyperstability if the non-linear block in the feedback path satisfies Popov's condition and the transfer matrix in the forward path of is strictly real positive (Zorgani et al., 2016).

Popov's criteria demand:

$$\int_0^t [\varepsilon]^T [W] dt \geq \gamma^2 \tag{14}$$

where $t \geq 0$ and γ represents a positive factor.

The error function ε is represented by a vector inner product that is not reliant on the frame of reference used to describe the vectors. You may use the following linearised expression to represent it:

The calculated speed is provided as:

$$\hat{\omega}_r = K_p \varepsilon + K_i \int \varepsilon dt \tag{15}$$

where the estimating error, represented by ε, is:

$$\varepsilon = \left(\hat{\psi}_{s\beta} \tilde{\psi}_{s\alpha} - \hat{\psi}_{s\alpha} \tilde{\psi}_{s\beta} - \left(\hat{i}_{s\alpha} \varepsilon_\beta - \hat{i}_{s\beta} \varepsilon_\alpha \right) \sigma L_s \right) \tag{16}$$

The whole MRAS-Super-twisting observer setup is shown in Figure 2.

Implementing the adaptive model is difficult due to the smooth integration of detected information being a requisite. This raises challenges in terms of the beginning conditions and drift. However, integrating low-pass filtering is advantageous since it helps in normalizing model outputs and in reducing high-frequency components often observed in motor voltages and currents (Schauder, 1992).

The K_p and K_i of the adaptation mechanism are given as defined in Tajima and Hori (1993)

$$\begin{cases} \boldsymbol{K}_P = \left(2\xi\omega_c - 1/T_s\right)/|\psi_s|^2 \\ K_I = \omega_c^2/|\psi_s|^2 \end{cases} \tag{17}$$

where ξ is the damping factor and ω_c is the natural angular frequency

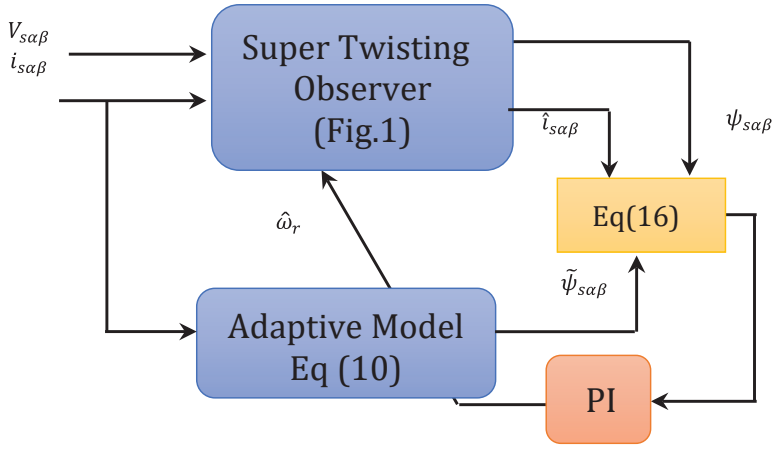

Figure 2. The combination of the stator flux model–MRAS speed observer and the super-twisting observer. MRAS, model reference adaptive system; PI, proportional-integral.

4. STFL Control

4.1. STFL flux and torque control design

The proposed approach integrates the feedback linearisation control rule with two independent super-twisting controllers. The combination of dual non-linear control approaches can manage system parameter uncertainties and deviations. As a result, this combination improves its performance and provides outstanding functioning in both the transitional and stable states.

The square of the stator flux magnitude and electromagnetic torque are the chosen control outputs (Ammar et al., 2020a; Orlowska-Kowalska et al., 2014). The purposes of control are identified as:

$$\begin{cases} y_1 = T_e = p(\psi_{s\alpha} i_{s\beta} - \psi_{s\beta} i_{s\alpha}) \\ y_2 = |\psi_s|^2 = \psi_{s\alpha}{}^2 + \psi_{s\beta}{}^2 \end{cases} \tag{18}$$

$$\begin{cases} e_1 = T_e^* - T_e \\ e_2 = |\psi_s^*|^2 - |\psi_s|^2 \end{cases} \tag{19}$$

where e_1, e_2: inaccuracies in torque and flux tracking.

The proposed super-twisting controllers produced the auxiliary inputs for the feedback linearisation controller and the input flux- and torque-sliding surfaces. The torque- and flux-sliding surfaces S_{Te} and $S_{\psi s}$ are given as:

$$\begin{cases} S_{T_e} = e_1 = T_e^* - T_e \\ S_{\psi_s} = e_2 = |\psi_s^*|^2 - |\psi_s|^2 \end{cases} \tag{20}$$

The torque and flux controllers for super twisting may be expressed as follows:

$$\begin{cases} \dot{V}_{T_e} = -\beta sign(S_{T_e}) \\ V_{ST1} = -\lambda |S_{T_e}|^{\rho} sign(S_{T_e}) + V_{T_e} \end{cases} \tag{21}$$

$$\begin{cases} \dot{V}_{\psi_s} = -\beta sign(S_{\psi_s}) \\ V_{ST2} = -\lambda |S_{\psi_s}|^{\rho} sign(S_{\psi_s}) + V_{\psi_s} \end{cases} \tag{22}$$

The stability analysis can be done using the proposed Lyapunov function presented in Moreno and Osorio (2012). In practical scenarios, the control system is influenced by various uncertainties, such as fluctuations in parameters, disturbances, and measurement inaccuracies. Thus, the dynamic control plant with disturbance can be written as :

$$\dot{x} = ax + bu + D \tag{23}$$

where x is the state (i.e. flux and torque), u is the input and D is the disturbance.

The stability analysis can be proved by a suitable Lyapunov candidate function V as presented in Barth et al. (2015)

$$V = \beta |S| + \frac{1}{2} V^2 \tag{24}$$

Considering that the system disturbance is bounded as:

$$D \le D_{\max} |S|^{0.5} \tag{25}$$

The time derivative of the Lyapunov function V can be written as:

$$\dot{V} \le \beta sign(S)\left(-\lambda |S|^{0.5} sign(S) + D_{\max} |S|^{0.5}\right) \tag{26}$$

Therefore, λ must be chosen greater than D_{max} ($\lambda > D_{max}$) in order to insure that $\dot{V}$ is negative definite, which guarantees that the system is asymptotically stable (Guo et al., 2019).

In practical applications, positive gains ensure stable system operation, similar to how it is done for a PI controller. The convergence time of the system is closely tied to the λ gain. Therefore, adjusting λ effectively controls the system's response time. However, large λ values can introduce ripples during the steady-state operation. On the other hand, the β gain affects the steady-state accuracy. The gain selection mechanism utilised has been described in detail in Lascu et al. (2019).

By using the feedback linearisation principle and the model shown in Eq. (1), the relationship between the input and the output may be driven as:

$$\dot{\mathbf{e}} = \begin{bmatrix} \dot{e}_1 \\ \dot{e}_2 \end{bmatrix} = \begin{bmatrix} F_1 \\ F_2 \end{bmatrix} + \mathbf{C}(x) \begin{bmatrix} V_{s\alpha} \\ V_{s\beta} \end{bmatrix} \tag{27}$$

with

$$\begin{cases} F_1 = -p\left[\mu(\psi_{s\alpha} i_{s\beta} - \psi_{s\beta} i_{s\alpha}) + \omega_r(\psi_{s\alpha} i_{s\alpha} - \psi_{s\beta} i_{s\beta}) - \dfrac{\omega_r}{\sigma L_s}|\psi_s|^2\right] \\ F_2 = 2R_s(\psi_{s\alpha} i_{s\alpha} - \psi_{s\beta} i_{s\beta}) \end{cases}$$

$$\mathbf{C}(x) = \begin{bmatrix} -p\left(i_{s\beta} - \dfrac{\psi_{s\beta}}{\sigma L_s}\right) & p\left(i_{s\alpha} - \dfrac{\psi_{s\alpha}}{\sigma L_s}\right) \\ -2\psi_{s\alpha} & 2\psi_{s\beta} \end{bmatrix}$$

The following is the expression for the determinant of the matrix C(x):

$$\det(\mathbf{C}(x)) = 2p\frac{M_{sr}}{\sigma L_s L_r}[\psi_{s\beta}\psi_{r\beta} + \psi_{s\alpha}\psi_{r\alpha}] \tag{28}$$

where $\psi_{r\alpha}$, $\psi_{r\beta}$ are elements of the rotor flux.

The system is linearisable as long as the matrix C(x) is not unique. The ultimate control rule of an STFL system when the super-twisting controller is entered as auxiliary inputs (i.e. reference voltages) is stated as:

$$\mathbf{V_s} = \begin{bmatrix} V_{s\alpha}^* \\ V_{s\beta}^* \end{bmatrix} = \mathbf{C}^{-1}(\mathbf{x}) \begin{bmatrix} -F_1 + V_{ST1} \\ -F_2 + V_{ST2} \end{bmatrix} \tag{29}$$

V_{ST1} and V_{ST2} are the recently developed super-twisted auxiliary inputs.

Figure 3 shows the proposed super-twisting-based auxiliary input to the feedback linearisation control.

4.2. Sensorless control stability

To create the inverter switching state under constant switching frequency, the space vector modulation unit will receive the final reference voltages ($V_{s\alpha}$, $V_{s\beta}$).

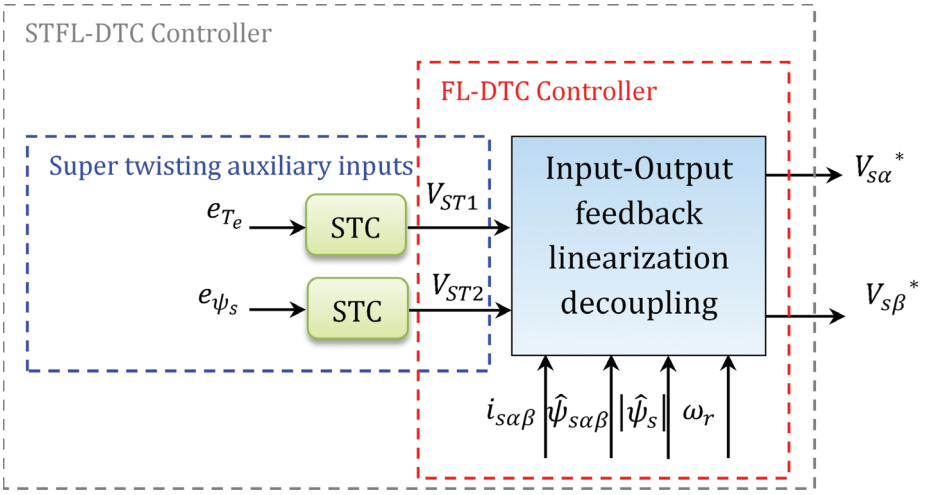

Figure 3. The combination of feedback linearisation and super-twisting auxiliary inputs. DTC, direct torque control; STFL, super twisting feedback linearisation.

In order to prevent singularities, the flux observer needs to be configured with beginning circumstances before using the sensorless control approach. In light of this, an offset is applied to the projected flow (Ghanes and Zheng, 2009). The estimated quantities (i.e. flux, torque and speed) will be substituted in the feedback linearisation control law. The hat (^) indication denotes the estimated quantities:

$$\mathbf{V_s}\left(\hat{\psi}_s,\hat{\mathrm{i}}_\mathrm{s},\hat{\omega}_r\right)=\begin{bmatrix}V_{s\alpha}^*\\V_{s\beta}^*\end{bmatrix}=\mathbf{C}^{-1}(\mathbf{x})\begin{bmatrix}-F_1+V_{ST1}\\-F_2+V_{ST2}\end{bmatrix} \tag{30}$$

with:

$$\begin{cases}F_1=-p\left[\mu(\hat{\psi}_{s\alpha}\hat{i}_{s\beta}-\hat{\psi}_{s\beta}\hat{i}_{s\alpha})+\hat{\omega}_r(\hat{\psi}_{s\alpha}\hat{i}_{s\alpha}-\hat{\psi}_{s\beta}\hat{i}_{s\beta})-\dfrac{\hat{\omega}_r}{\sigma L_s}|\psi_s|^2\right]\\F_2=2R_s(\hat{\psi}_{s\alpha}\hat{i}_{s\alpha}-\hat{\psi}_{s\beta}\hat{i}_{s\beta})\end{cases}$$

$$\mathbf{C}(x)=\begin{bmatrix}-p\left(\hat{i}_{s\beta}-\dfrac{\hat{\psi}_{s\beta}}{\sigma L_s}\right) & p\left(\hat{i}_{s\alpha}-\dfrac{\hat{\psi}_{s\alpha}}{\sigma L_s}\right)\\-2\hat{\psi}_{s\alpha} & 2\hat{\psi}_{s\beta}\end{bmatrix}$$

4.3. Speed control loop

The used PI controller in the outer speed loop for all control schemes is the anti-windup controller. The transfer function (TF) using Laplace transform of the speed loop is given as following:

$$G_{\omega_r}(s)=\frac{\omega_r(s)}{T_e(s)-T_L(s)}=\frac{1}{Js+f} \tag{31}$$

The TF of the PI controller is defined as follows:

$$PI=K_p s+\frac{K_i}{s} \tag{32}$$

where K_p and K_i are the proportional and integral gains.

By considering the load torque TL as a disturbance. The global TF of the speed control in open loop becomes:

$$G_{\omega_r}(s) = \frac{\omega_r(s)}{\omega_r^*(s)} = \frac{1}{Js+f}\left(K_p s + \frac{K_i}{s}\right) \tag{33}$$

Using the poles placement method, the controller's gains can be given as:

$$\begin{cases} K_i = J\omega_n^2 \\ K_p = 2\xi\omega_n J - f \end{cases} \tag{34}$$

where ω_n is the natural frequency and ξ is the damping coefficient

Figure 4 displays the global diagram of the MRAS-super-twisting observer-based sensorless control system using super-twisting-feedback linearisation.

5. Simulation and Experimental Results

Using MATLAB/Simulink software and the dSpace 1104 real-time interface, simulation and experimental validation have been used to validate the proposed sensorless control based on super twisting. Table 1

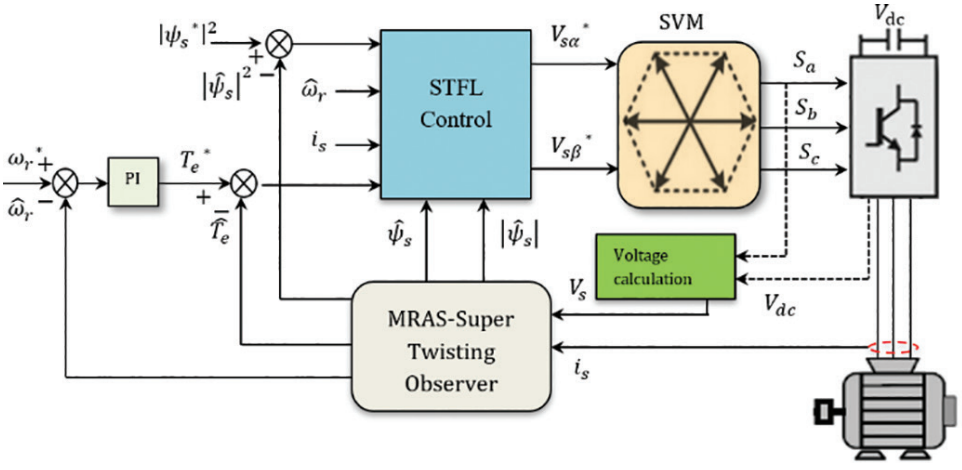

Figure 4. Sensorless STFL-direct flux and torque control block diagram using MRAS-super-twisting observer. MRAS, model reference adaptive system; PI, proportional-integral; STFL, super-twisting feedback linearisation.

Table 1. Induction motor characteristics.

Parameters	Symbol	Value	Unit
Machine's power	P	1.1	kW
Rated voltage	Vs	220/380	V
Rated speed	N	1,500	rpm
Stator resistance	Rs	6.75	Ω
Rotor resistance	Rr	6.21	Ω
Stator inductance	Ls	0.5192	H
Rotor inductance	Lr	0.5192	H
Mutual inductance	Msr	0.4957	H
Number of pole pairs	P	2	–
The moment of inertia	J	0.01240	kg · m^{-2}
Friction coefficient	F	0.002	SI

contains data related to the investigation of the simulation and experimental implementation for a 1.1 kW induction motor.

5.1. Simulation results

The following simulation results examine the suggested second-order SMO for MRAS (MRAS-STO)'s performance analysis. The figures illustrate several tests performed to assess the robustness and the suggested observer's estimate accuracy, like turning on, steady-state and low-speed operation. An observer proposal is contrasted with a first-order SMO structure using a speed estimator in an open loop (OLSE-SMO) that is presented in Ammar et al. (2020b), where (a) is for the first-order SMO and (b) is for the MRAS-associated super-twisting observer.

In response to a step input of 1,000 rpm without a load, the motor speed response and estimation errors are shown in Figure 5. Good superposition of the two speed variables for both observers is evident. The first-order SMO (Figure 5(a)) displays a significant estimation error during the transient state and a smaller error during the stable state. On the other hand, the MRAS-based super-twisting observer (ST-MRAS) provided more accurate estimations, which corresponds to a quicker error convergence. Furthermore, this observer may remove the error across both steady-state and transient scenarios.

Figures 6 and 7 show the stator flux's progression. The plot depicts the flux magnitude and axis components for both observers. All observers display an accurate estimation and reduced disturbance since the control algorithm predetermines the stator flux amount (Figure 7). Furthermore, Figure 7 shows the stator flux elements throughout a test of speed reversal. The flux evolution exhibits a pure sinusoidal waveform as a result of the direct flux control that is being suggested. The location of flux shown below illustrates the speed direction reversing.

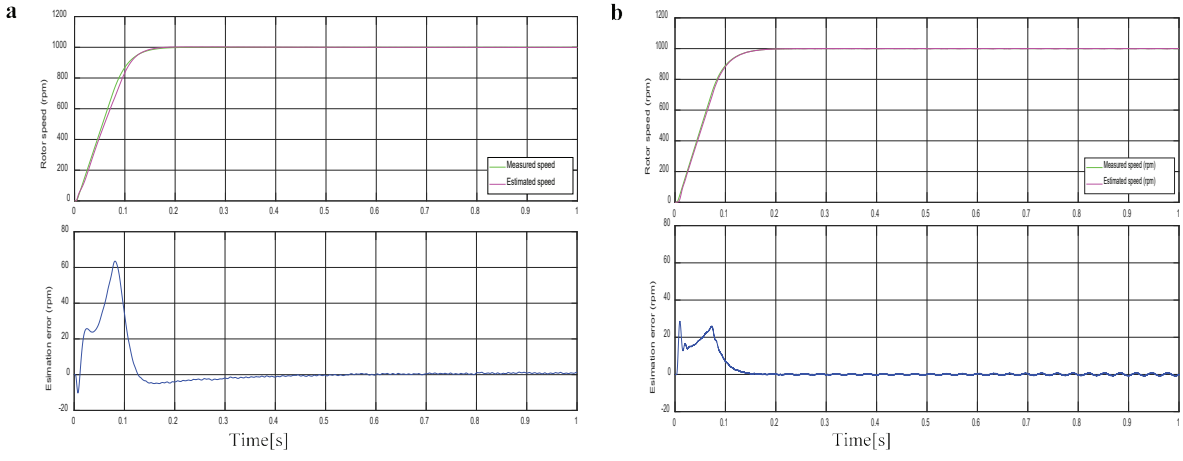

Figure 5. Getting started: measured and estimated speed, estimation error (a: SMO; b: ST-MRAS).

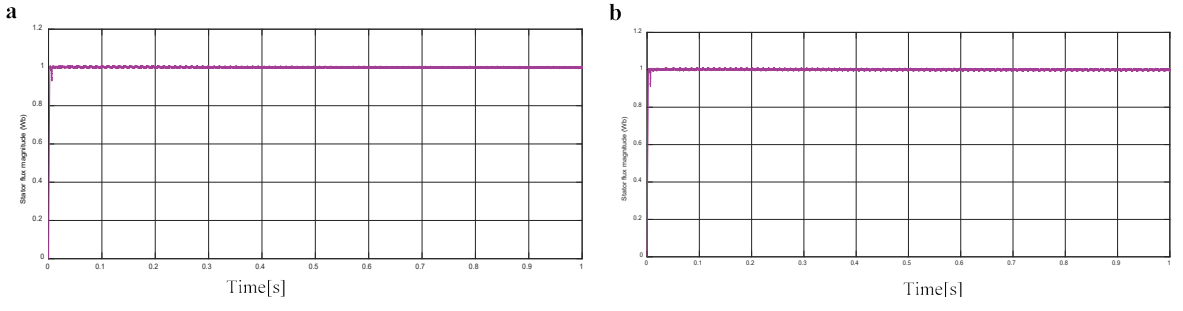

Figure 6. Stable state: stator flux magnitude (a: SMO; b: ST-MRAS).

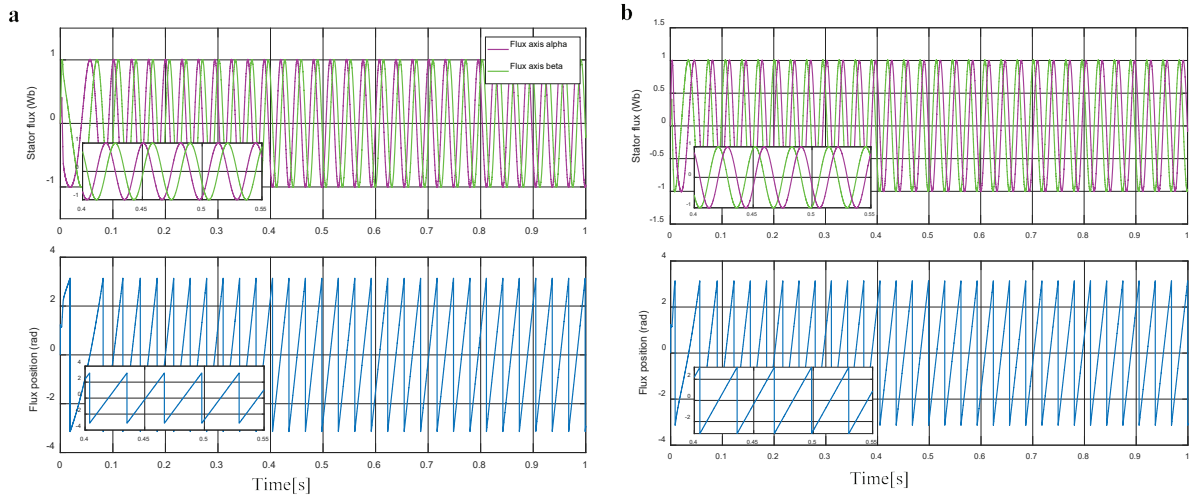

Figure 7. Stable state and sense reversal: Stator flux components, flux position (a: SMO; b: ST-MRAS).

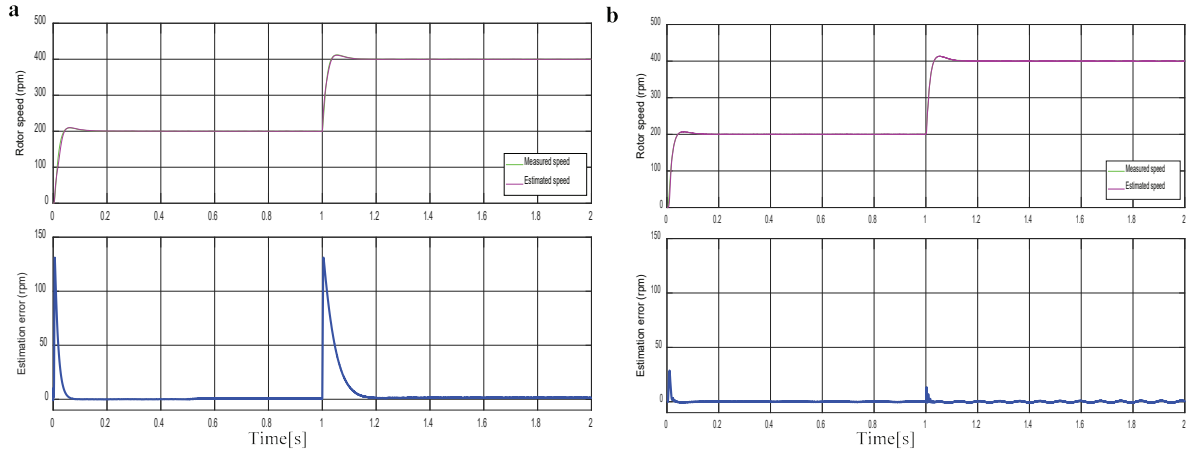

Figure 8. Operation at low speed: 200–400 rpm measured and estimated speed, estimation error (a: SMO; b: ST-MRAS).

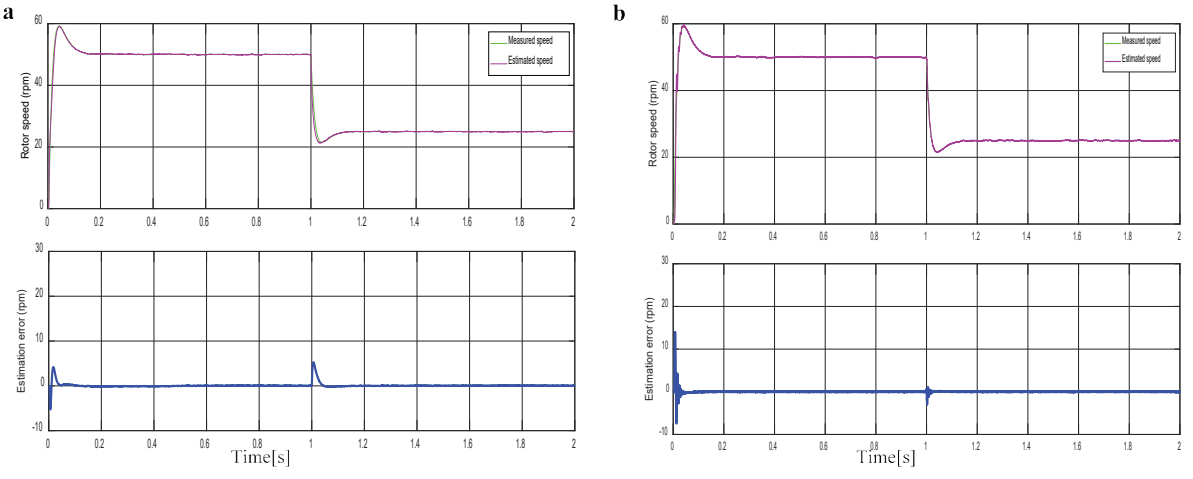

Figure 9. Reduced speed operation: 50–25 rpm measured and estimated speed, estimation error (a: SMO; b: ST-MRAS).

Next, low-speed operating experiments have been performed, with a speed reference varying between 200–400 rpm and 50–25 rpm, as depicted separately in Figures 8 and 9. Both observers show a slight overshoot at the start (Figure 8) but it has been recovered shortly. This overshoot depends on the speed controller used for the speed loop. As can be shown, the corresponding MRAS super-twisting observer in Figures 8 and 9(b) has more accurate superposition between speed quantities and better estimate. The estimation errors shown at the bottom validate these observations in Figures 8 and 9(a, b). The adaptive observer has higher error during slow convergence and higher error during transient states. Moreover, in the very low speed zone in Figure 9 (50–25 rpm), the super-twisting observer maintains the estimation accuracy and shows no speed variations; in addition, control stability is preserved.

Figures 10 and 11 show the speed reversing and zero speed tests. In both the tests, the observers show stable speed estimation at zero speed/frequency (0 rmp; 0 Hz). However, the associated super-twisting observer was more accurate; it can be seen that the speed value is correct even when the machine stops rotation.

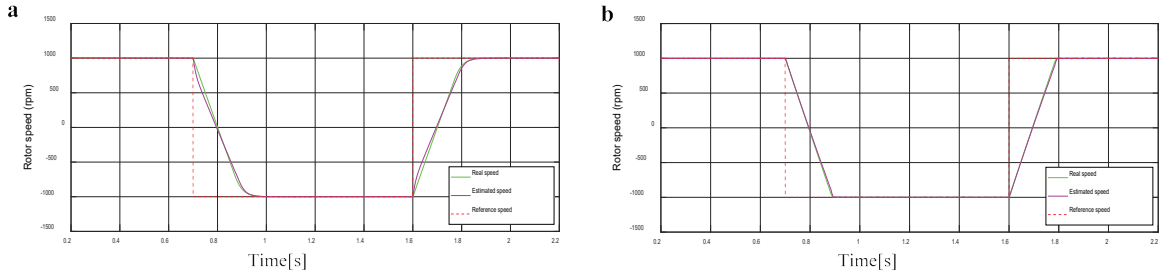

Figure 10. Speed reversal test: 1,000; –1,000 rpm measured and estimated speed (a: SMO; b: ST-MRAS).

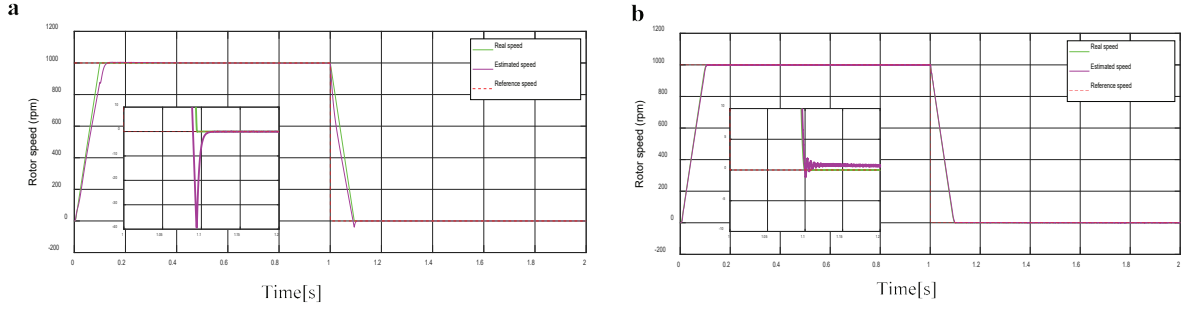

Figure 11. Zero speed: 1,000–0 rpm measured and estimated speed (a: SMO; b: ST-MRAS).

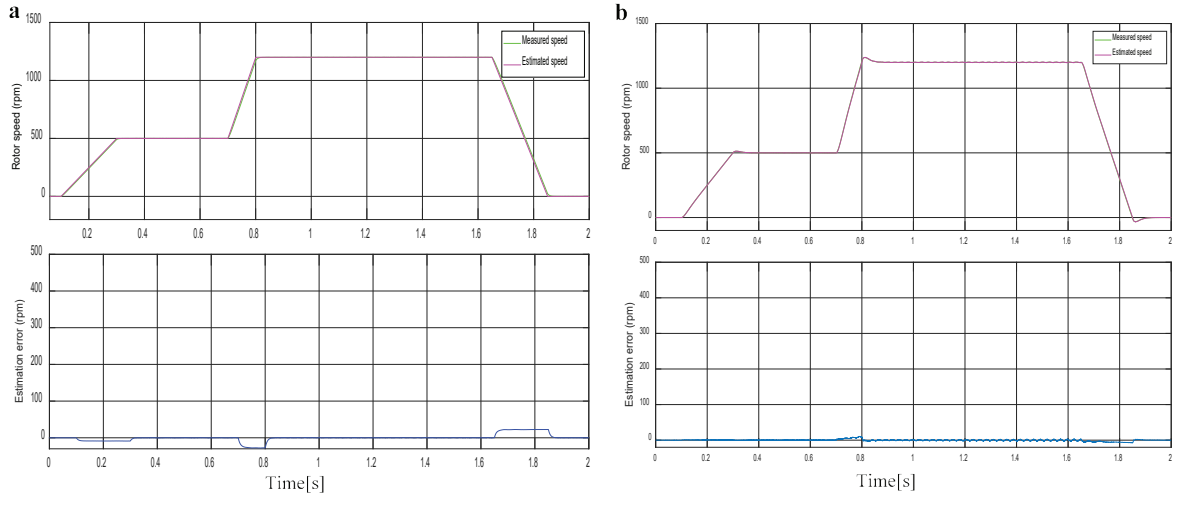

Figure 12. Zero speed: 1,000–0 rpm measured and estimated speed (a: SMO; b: ST-MRAS).

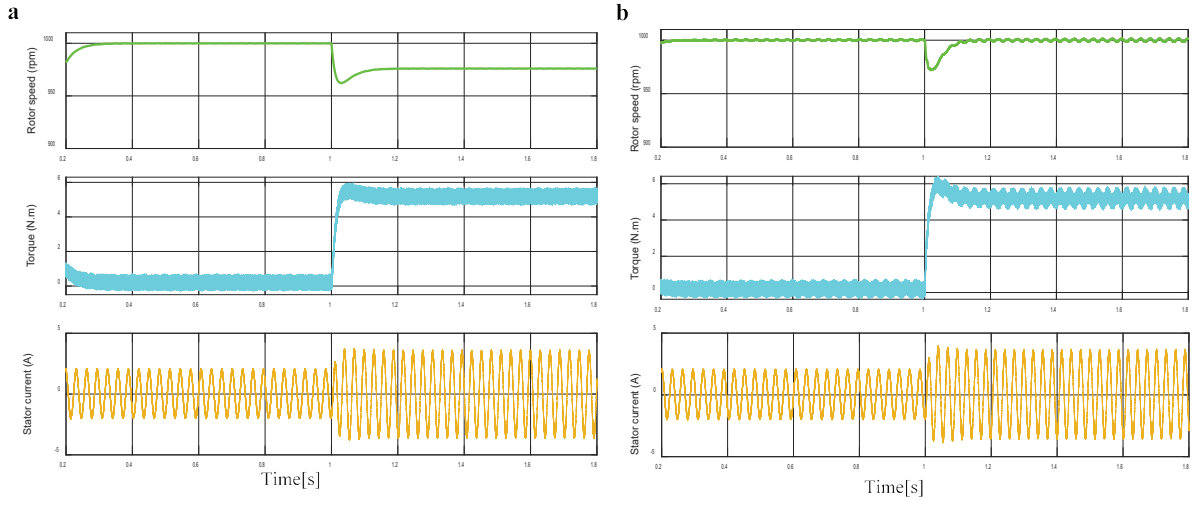

Figure 13. Load application test: rotor speed, torque, stator current (a: SMO; b: ST-MRAS).

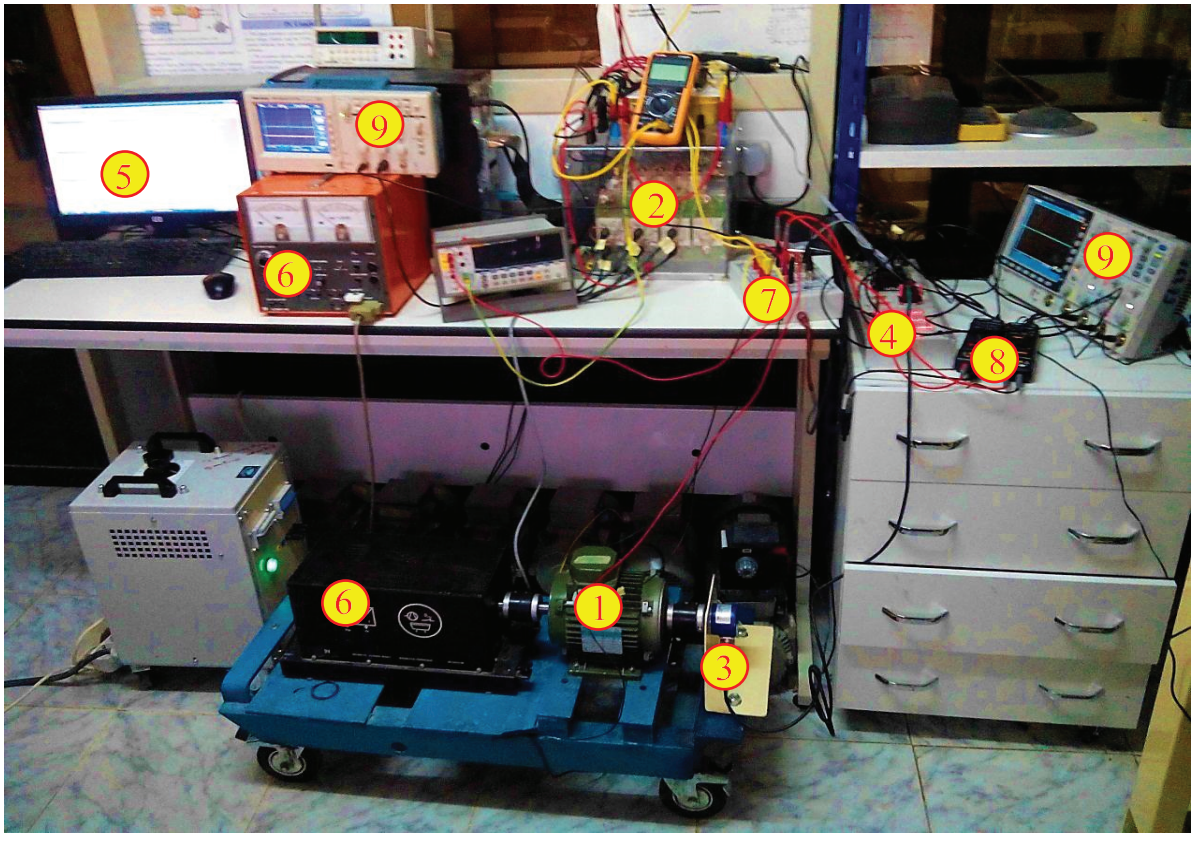

Figure 14. Test bench description.

Lastly, a variable speed test is shown in Figure 12. This test, which shows the rotor speed estimate and estimation errors from zero to medium speed (500 rpm) and finally to high speed (1,200 rpm), can include all of the tests that came before it. As seen in Figure 12(a), the adaptive observer exhibits substantial inaccuracy during the steady state. However, it is apparent that the suggested super-twisting observer has a connection to MRAS. It allows for

reduced estimate error in dynamic state operations, extremely fast convergence in stable state and good estimation and perfect speed superposition during the instantaneous speed changes. Figure 13 displays the load application test, with the rotor speed, torque and stator current represented from top to bottom. In Figure 13(b), the speed loop with the MRAS-based super-twisting observer demonstrates higher load disturbance rejection compared with the case of the classical SMO. We may also observe the fast torque response and the current increase while the load is being applied.

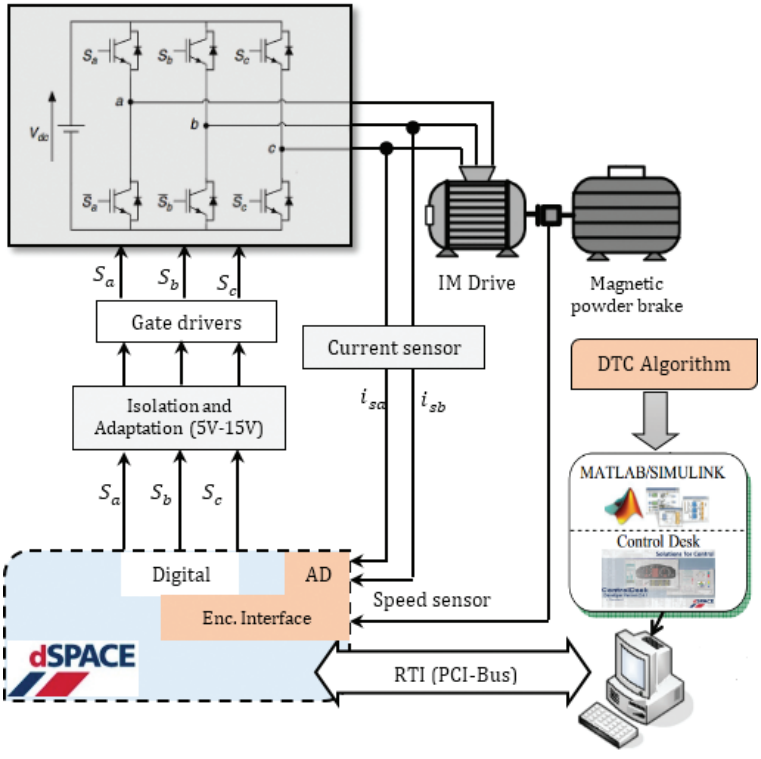

Figure 15. Descriptive diagram. DTC, direct torque control.

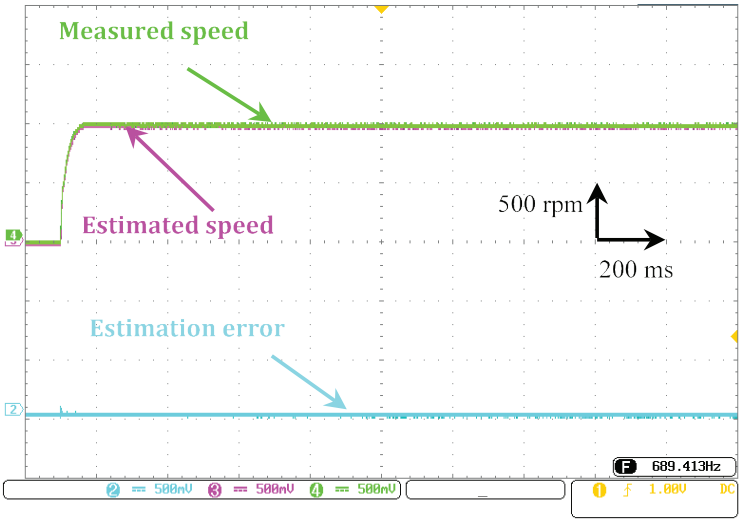

Figure 16. Starting up: estimated and measured speed, estimation inaccuracy.

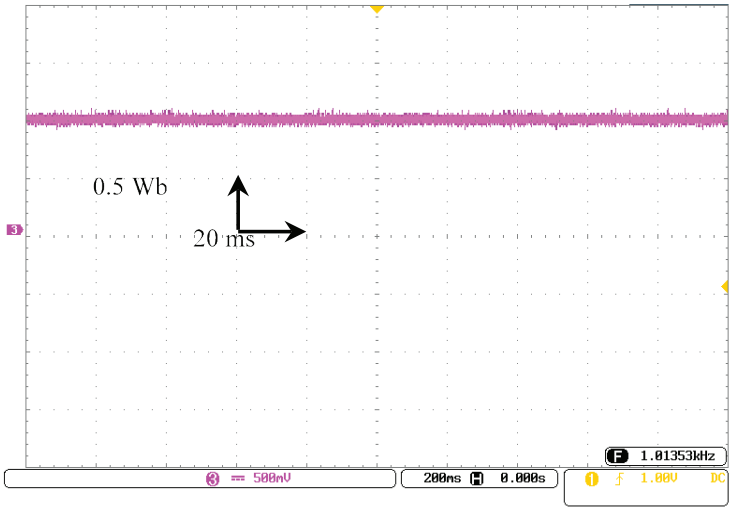

Figure 17. Stable state: stator flux magnitude.

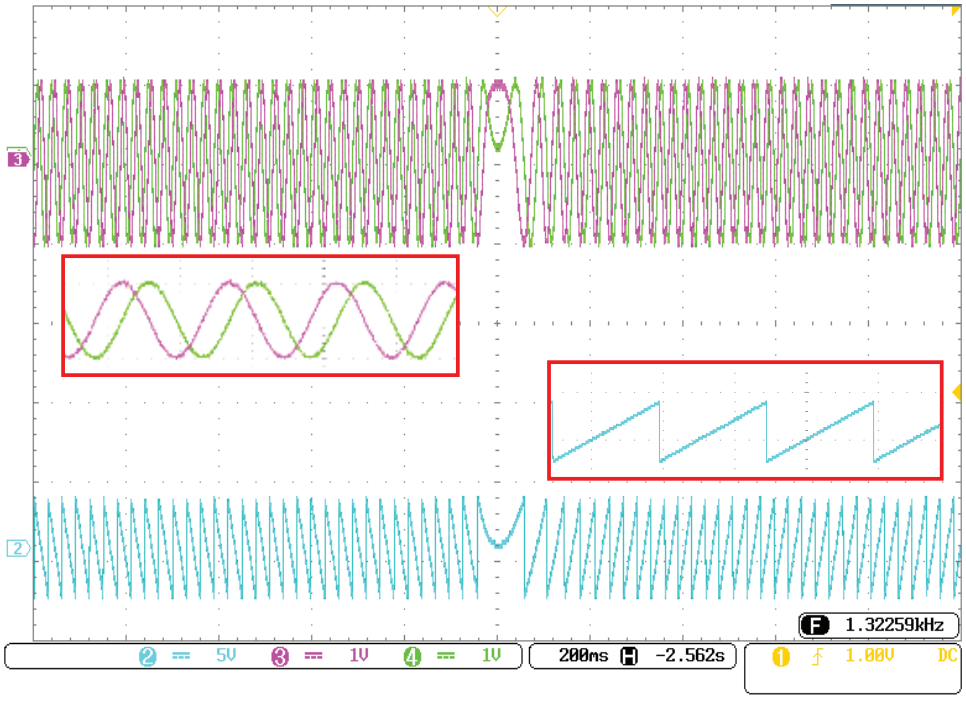

Figure 18. Reversal of speed sense: stator flux components and flux position.

5.2. Experimental setup

The experimental validation of the suggested super-twisting second-order SMO using MRAS is covered in this section. MATLAB/Simulink software with a dSpace 1104 real-time interface has been used to achieve STFL with a super-twisting observer.

The experimental test bench depicted in Figure 14 consists of 1: A squirrel-cage induction machine rated at 1.1 kW., 2: voltage converter with two levels of power electronics, 3: a sequential encoder, 4: real-time interface dSpace 1104, 5: MATLAB/Simulink/ControlDesk programme on staff computer, 6: magnetic powder braking

system, 7: Current Hall effect sensors, and 8: voltage detectors, and 9: the oscilloscope analogue. The rest of the details concerning the experimental setup have been mentioned in the appendix section.

Figure 15 depicts the software and hardware interconnection.

5.3. Experimental results

The following figures provide several speed tests conducted to assess the observer's ability over a wide speed range. The same circumstances are considered as in the previous simulation section.

The experimental findings of the starting up test are shown in Figure 16. Two-speed numbers with estimation error (measured speed with an encoder and estimated speed using STO) are displayed. Both speed numbers are in good superposition, as shown in the simulation section, and the estimation error converges to zero. The amount, components and position of the stator flux are then shown in Figures 17 and 18. With a decent waveform, the flux follows its reference. This shows the accuracy of the estimation.

Figures 19 and 20 show the low-speed functioning. The estimated and observed speed values are fully superposed, although the estimation error converges to zero in the low-speed and extremely load-speed

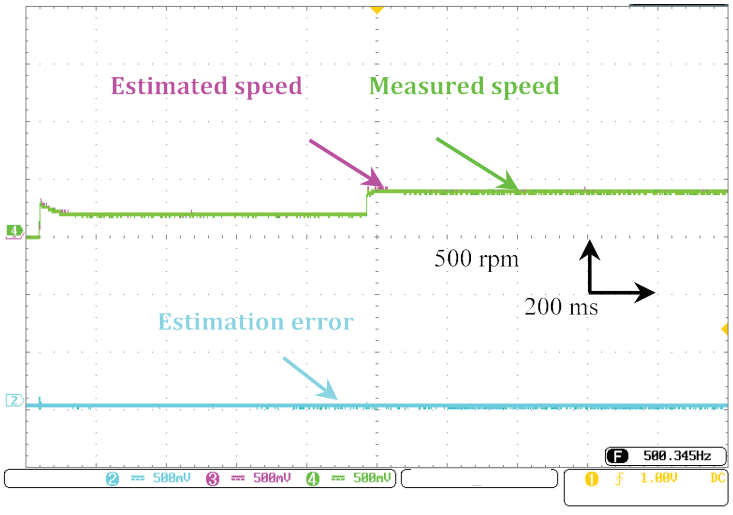

Figure 19. Operation at low speeds: measured and estimated speed (200–400 rpm), estimation error.

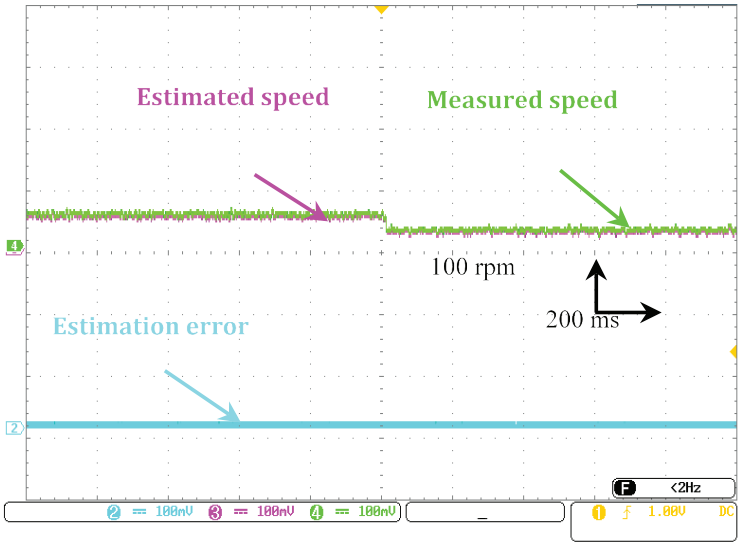

Figure 20. Operation at low speeds: measured and estimated speed (50–25 rpm), estimation error.

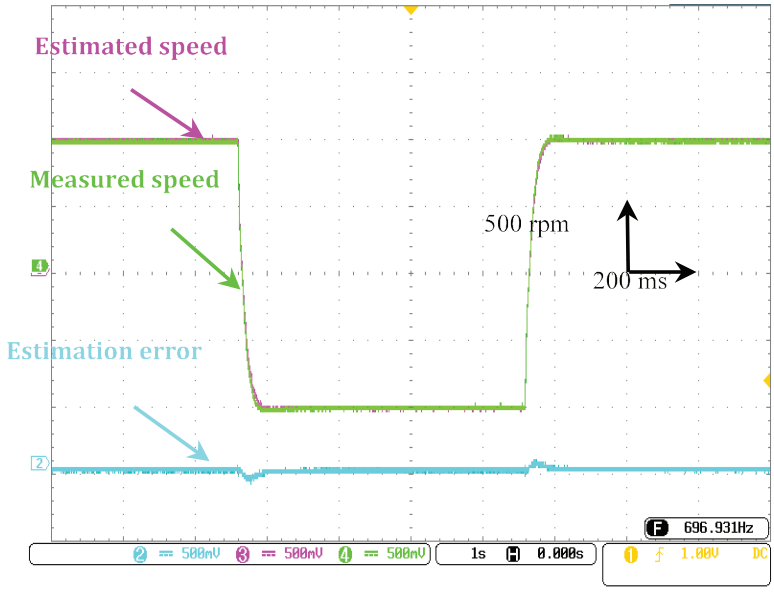

Figure 21. Speed reversal test: 1,000; –1,000 rpm measured and estimated speed.

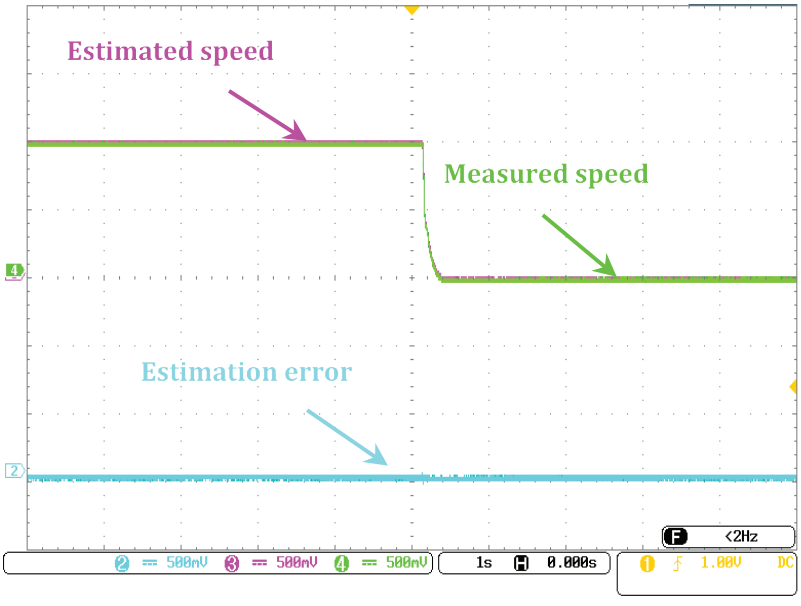

Figure 22. Zero speed: 1,000–0 rpm measured and estimated speed.

regions. The estimating accuracy has not changed, the speed has not changed and the control stability has not changed.

Figures 21 and 22 show the speed reversing test and zero speed operation. In both tests, the proposed observer shows its height resilience and accuracy under difficult conditions. This can be proved from the estimation error that stayed around zero during all operation points. An industrial benchmark speed profile is employed in the final test shown in Figure 23. It comprises all of the speed tests from a large area. It can be seen that the proposed MRAS-STO observer has a highly accurate estimation for both steady-state and sudden speed changes.

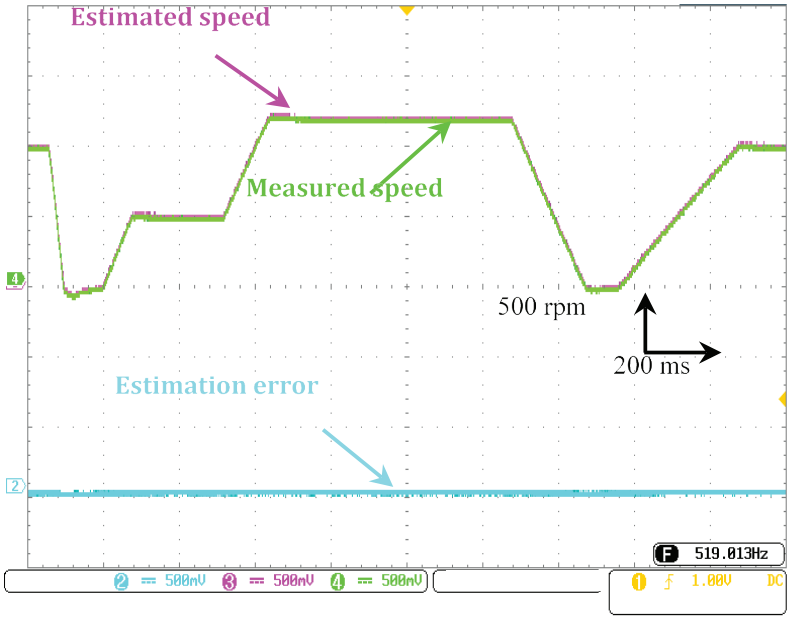

Figure 23. Operation at variable speeds: measured and estimated speed, estimation error.

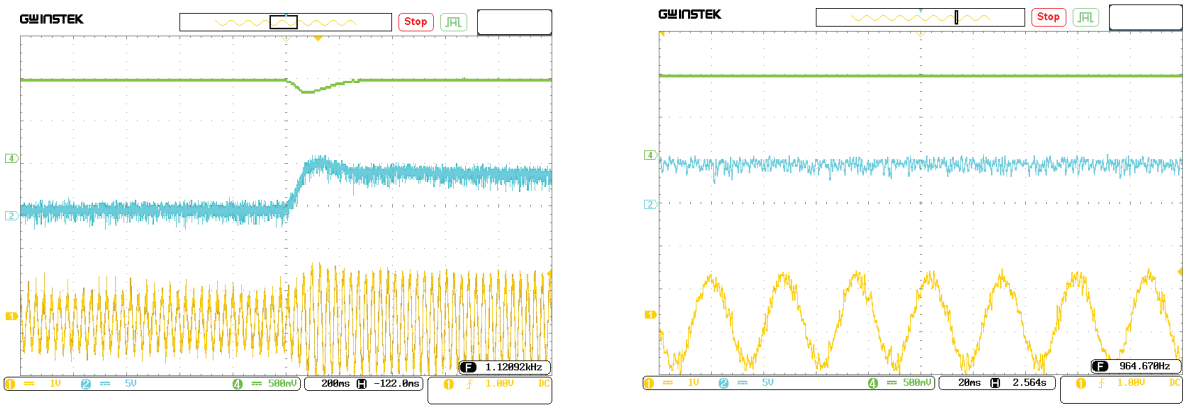

Figure 24. Load experimental test with zoom of: rotor speed, torque, stator current (with ZOOM).

The experimental test confirmed our simulation's findings, demonstrating that the MRAS super-twisting observer exhibits a higher load disturbance rejection and a more effective response in achieving the reference speed after load application, as illustrated in Figure 24.

6. Conclusion

The present paper presents a revolutionary performance boost for induction motor flux and torque management using dual non-linear control approaches. The combined control strategy has been used to address the various shortcomings of the traditional control systems. The decoupled control has been implemented, and the reference voltages are generated using a feedback linearisation technique. The super-twisting approach was then employed as a supporting auxiliary control to achieve the so-called robust feedback linearisation control.

Furthermore, the proposed super-twisting observer coupled with the MRAS has been tested and demonstrates outstanding estimation accuracy in various speed zones that represent the total system dependability and cost. The suggested technique was tested under various operating conditions utilising simulation and experimental implementation in dSpace 1104. In general, using continuous super twisting for control and estimation results in less chattering, faster dynamics, higher resilience and better estimate over a wide speed range. Furthermore, the control design has been maintained as simple as feasible; this feature makes it executable in more cost-effective microcontrollers rather than dSpace 1104, such as C2000 Texas instrument microcontroller and STM32.

Declaration of conflicting interests

The author(s) declared no potential conflicts of interest with respect to the research, authorship and/or publication of this article.

Funding

The author(s) received no financial support for the research, authorship and/or publication of this article.

References

Ammar, A., Ameid, T., Azzoug, Y., Kheldoun, A. and Metidji, B. (2020a). Design of speed sensorless control of induction motor based on dual-nonlinear control technique. In: *s International Conference on Electrical Engineering (ICEE)*. Istanbul, Turkey: IEEE, pp. 1–6.

Ammar, A., Kheldoun, A., Metidji, B., Ameid, T. and Azzoug, Y. (2020b). Feedback Linearization Based Sensorless Direct Torque Control using Stator Flux MRAS-Sliding Mode Observer for Induction Motor Drive. *ISA Transactions*, 98, pp. 382–392. doi: 10.1016/j.isatra.2019.08.061.

Barambones, O., Alkorta, P. and de Durana, J. M. G. (2014). A Real-Time Estimation and Control Scheme for Induction Motors Based on Sliding Mode Theory. *Journal of the Franklin Institute*, 351(8), pp. 4251–4270. doi: 10.1016/j.jfranklin.2014.04.020.

Barth, A., Reichhartinger, M., Regern, J., Horn, M. and Wulff, K. (2015). Lyapunov-Design for a Super-Twisting Sliding-Mode Controller using the Certainty-Equivalence Principle. *IFAC-PapersOnLine*, 48(11), pp. 860–865. doi: 10.1016/j.ifacol.2015.09.298.

Bendjeddou, Y., Deboucha, A., Bentouhami, L., Merabet, E. and Abdessemed, R. (2021). Super Twisting Sliding Mode Approach Applied to Voltage Orientated Control of a Stand-Alone Induction Generator. *Protection and Control of Modern Power Systems*, 6(1), p. 18. doi: 10.1186/s41601-021-00201-2.

Choi, A., Kim, H., Hu, M., Kim, Y., Ahn, H. and You, K. (2022). Super-Twisting Sliding Mode Control with SVR Disturbance Observer for PMSM Speed Regulation. *Applied Sciences*, 12(21), p. 10749. doi: 10.3390/app122110749.

Csizmadia, M. and Kuczmann, M. (2023). A Novel Feedback Linearisation Control of Flyback Converter. *Power Electronics and Drives*, 8(1), pp. 74–83. doi: 10.2478/pead-2023-0006.

Czyżniewski, M. and Łangowski, R. (2024). Robust Asymptotic Super Twisting Sliding Mode Observer for Non-Linear Uncertain Biochemical Systems. *Journal of Process Control*, 136, p. 103192. doi: 10.1016/j.jprocont.2024.103192.

Ghanes, M. and Zheng, G. (2009). On Sensorless Induction Motor Drives: Sliding-Mode Observer and Output Feedback Controller. *IEEE Transactions on Industrial Electronics*, 56(9), pp. 3404–3413. doi: 10.1109/TIE.2009.2026387.

Guedida, S., Tabbache, B., Benzaoui, K. M. S., Nounou, K. and Nesr, M. (2024). Novel Speed Sensorless DTC Design for a Five-Phase Induction Motor with an Intelligent Fractional Order Controller Based-MRAS Estimator. *Power Electronics and Drives*, 9(1), pp. 63–85. doi: 10.2478/pead-2024-0005.

Guo, B., Su, M., Sun, Y., Wang, H., Dan, H., Tang, Z. and Cheng, B. (2019). A Robust Second-Order Sliding Mode Control for Single-Phase Photovoltaic Grid-Connected Voltage Source Inverter. *IEEE*

Access, 7, pp. 53202–53212. doi: 10.1109/ACCESS.2019.2912033.

Holakooie, M. H., Ojaghi, M. and Taheri, A. (2019). Modified DTC of a Six-Phase Induction Motor with a Second-Order Sliding-Mode MRAS-Based Speed Estimator. *IEEE Transactions on Power Electronics*, 34(1), pp. 600–611. doi: 10.1109/TPEL.2018.2825227.

Huang, G., Huang, W., Li, Z., Li, J., He, J., Zhang, C. and Zhao, K. (2021). An Improved Sliding-Mode Observer-Based Equivalent-Input-Disturbance Approach for Permanent Magnet Synchronous Motor Drives with Faults in Current Measurement Circuits. *Transactions of the Institute of Measurement and Control*, 43(12), pp. 2589–2598. doi: 10.1177/01423312211002584.

Lascu, C., Argeseanu, A. and Blaabjerg, F. (2019). Super-Twisting Sliding Mode Direct Torque and Flux Control of Induction Machine Drives. *IEEE Transactions on Power Electronics*, 35(5), pp. 5057–5065. doi: 10.1109/TPEL.2019.2944124.

Lascu, C., Boldea, I. and Blaabjerg, F. (2009). A Class of Speed-Sensorless Sliding-Mode Observers for High-Performance Induction Motor Drives. *IEEE Transactions on Industrial Electronics*, 56(9), pp. 3394–3403. doi: 10.1109/TIE.2009.2022518.

Levant, A. (2003). Higher-Order Sliding Modes, Differentiation and Output-Feedback Control. *International Journal of Control*, 76(9–10), pp. 924–941. doi: 10.1080/0020717031000099029.

Li, G., Li, H., He, X. and Wang, X. (2023). A Sensorless Control System of Permanent Magnet Synchronous Motor for Electric Locomotive Based on Improved High-Frequency Rotating Injection Method. *Transactions of the Institute of Measurement and Control*, 45(9), pp. 1685–1692. doi: 10.1177/01423312221142972.

Mao, S., Tao, H. and Zheng, Z. (2020). Sensorless Control of Induction Motors Based on Fractional-Order Linear Super-Twisting Sliding Mode Observer with Flux Linkage Compensation. *IEEE Access*, 8, pp. 172308–172317. doi: 10.1109/ACCESS.2020.3024626.

Moreno, J. A. and Osorio, M. (2012). Strict Lyapunov Functions for the Super-Twisting Algorithm. *IEEE Transactions on Automatic Control*, 57(4), pp. 1035–1040. doi: 10.1109/TAC.2012.2186179.

Orlowska-Kowalska, T., Tarchala, G. and Dybkowski, M. (2014). Sliding-Mode Direct Torque Control and Sliding-Mode Observer with a Magnetizing Reactance Estimator for the Field-Weakening of the Induction Motor Drive. *Mathematics and Computers in Simulation*, 98, pp. 31–45. doi: 10.1016/j.matcom.2013.05.012.

Qian, W., Li, W., Guo, X. and Wang, H. (2024). A Switching Gain Adaptive Sliding Mode Observer for SoC Estimation of Lithium-Ion Battery. *Energy*, 292, p. 130585. doi: 10.1016/j.energy.2024.130585.

Rashed, M., Goh, K. B., Dunnigan, M. W., MacConnell, P. F. A., Stronach, A. F. and Williams, B. W. (2005). Sensorless Second-Order Sliding-Mode Speed Control of a Voltage-Fed hInduction-Motor Drive Using Nonlinear State Feedback. *IEE Proceedings - Electric Power Applications*, 152(5), p. 1127. doi: 10.1049/ip-epa:20050042.

Sami, I., Ullah, S., Basit, A., Ullah, N. and Ro, J. (2020). Integral Super Twisting Sliding Mode Based Sensorless Predictive Torque Control of Induction Motor. *IEEE Access*, 8, pp. 186740–186755. doi: 10.1109/ACCESS.2020.3028845.

Schauder, C. (1992). Adaptive Speed Identification for Vector Control of Induction Motors Without Rotational Transducers. *IEEE Transactions on Industry Applications*, 28(5), pp. 1054–1061. doi: 10.1109/28.158829.

Tajima, H. and Hori, Y. (1993). Speed Sensorless Field-Orientation Control of the Induction Machine. *IEEE Transactions on Industry Applications*, 29(1), pp. 175–180. doi: 10.1109/28.195904.

Tang, Q., Shen, A., Luo, X. and Xu, J. (2017). PMSM Sensorless Control by Injecting HF Pulsating Carrier Signal Into ABC Frame. *IEEE Transactions on Power Electronics*, 32(5), pp. 3767–3776. doi: 10.1109/TPEL.2016.2583787.

Tarchala, G. and Orlowska-Kowalska, T. (2018). Equivalent-Signal-Based Sliding Mode Speed MRAS-Type Estimator for Induction Motor Drive Stable in the Regenerating Mode. *IEEE Transactions on Industrial Electronics*, 65(9), pp. 6936–6947. doi: 10.1109/TIE.2018.2795518.

Vajsz, T., Számel, L. and Handler, Á. (2019). An Investigation of Direct Torque Control and Hysteresis Current Vector Control for Motion Control Synchronous Reluctance Motor Applications. *Power Electronics and Drives*, 4(1), pp. 115–124. doi: 10.2478/pead-2019-0009.

Wang, F., Zhang, Z., Mei, X., Rodríguez, J. and Kennel, R. (2018a). Advanced Control Strategies of Induction Machine: Field Oriented Control, Direct Torque Control and Model Predictive Control. *Energies*, 11(1), p. 120. doi: 10.3390/en11010120.

Wang, H., Ge, X. and Liu, Y.-C. (2018b). Second-Order Sliding-Mode MRAS Observer-Based Sensorless Vector Control of Linear Induction Motor Drives

for Medium-Low Speed Maglev Applications. *IEEE Transactions on Industrial Electronics*, 65(12), pp. 9938–9952. doi: 10.1109/TIE.2018.2818664.

Wu, T., Luo, D., Wu, X., Liu, K., Huang, S. and Peng, X. (2021). Square-wave Voltage Injection Based PMSM Sensorless Control Considering Time Delay at Low Switching Frequency. *IEEE Transactions on Industrial Electronics*, 69(6), pp. 5525–5535. doi: 10.1109/TIE.2021.3094444.

Xin, Z., Zhao, R., Blaabjerg, F., Zhang, L. and Loh, P. C. (2017). An Improved Flux Observer for Field-Oriented Control of Induction Motors Based on Dual Second-Order Generalized Integrator Frequency-Locked Loop. *IEEE Journal of Emerging and Selected Topics in Power Electronics*, 5(1), pp. 513–525. doi: 10.1109/JESTPE.2016.2623668.

Zorgani, Y. A., Koubaa, Y. and Boussak, M. (2016). MRAS State Estimator for Speed Sensorless ISFOC Induction Motor Drives with Luenberger Load Torque Estimation. *ISA Transactions*, 61, pp. 308–317. doi: 10.1016/j.isatra.2015.12.015.

Appendix

The sampling frequency: 10 kHz.
Inverter's switching frequency: 5 kHz.
DC link voltage: Vdc = 537 V.